JAERI-Conf 2001-002

ICANS-XV
15^{th} Meeting of the International Collaboration on Advanced Neutron Sources
November 6-9, 2000
Tsukuba, Japan

20.4
Spallation Reactions and Energy Deposition in Heavy Target Materials Comparison of Measurements and MC-Calculations

D.Filges[a] *, M.Enke[c], J.Galin[b], F.Goldenbaum[a], C-M.Herbach[c], D.Hilscher[c], U.Jahnke[c], A.Letourneau[b], B.Lott[b], R.-D. Neef[a], K.Nünighoff[a], N.Paul[a], A.Péghaire[b], L.Pienkowski[d], C.Pohl[a], H.Schaal[a], U.Schröder[e], G.Sterzenbach[a], A.Tietze[f], V.Tishchenko[c], J.Toke[e], M.Wohlmuther[a]

[a] *Forschungszentrum Jülich GmbH, Institut für Kernphysik, D-52425 Jülich, Germany*
[b] *GANIL, BP 5027, F-14076 Caen Cedex 5, France*
[c] *Hahn-Meitner Institut Berlin GmbH, Glienickerstr.100, D-14109 Berlin, Germany*
[d] *Heavy Ion Laboratory Warsaw University, Pasteura 5a, 02-093 Warszawa, Poland*
[e] *University of Rochester, Rochester, New York 14627, USA*
[f] *Universität Wuppertal, 42329 Wuppertal, Germany*

(November 28, 2000)

A renascence of interest for energetic proton induced production of neutrons originates recently by the inception of new projects for target stations of intense spallation neutron sources (like the planned European Spallation Source ESS), accelerator-driven nuclear reactors, nuclear waste transmutation and also the application for radioactive beams. Here we verify the predictive power of transport codes currently on the market by confronting observables and quantities of interest with an exhaustive matrix of benchmark data essentially coming from two experiments being performed at the Cooler Synchrotron COSY at Jülich . Program packages like HERMES, LCS or MCNPX master the prevision of reaction cross sections, hadronic interaction lengths, averaged neutron multiplicities and neutron multiplicity distributions in thick and thin(!) targets for a wide spectrum of incident proton energies, geometrical shapes and materials of the target. While also the observables related to the energy deposition in thick targets are in a good agreement with the model predictions, the production cross section measurements however for light charged particles on thin targets point out that problems exist within these models.

I. INTRODUCTION

A recurrence of interest for energetic proton induced production of neutrons originates recently by the inception of new projects for target stations of intense neutron spallation sources [1], accelerator-driven nuclear reactors nuclear waste transmutation and also the application for radioactive beams or the production of tritium (APT project in the US).

In this framework the most important question is to determine the most efficient way to convert the primary beam energy into neutron production. Although the task has been quite successfully investigated experimentally by varying the incident proton energy for various target materials and a huge collection of different target geometries—providing an exhaustive matrix of benchmark data—the ultimative ambition is to increase the predictive power of transport codes currently on the market.

In the present paper we will essentially present two sets of experimental data. In the first part reaction cross sections, hadronic interaction lengths, averaged neutron multiplicities, neutron multiplicity as well as charged particle cross sections being measured within the NESSI campaign are investigated in order to validate codes considered in the present contribution. Unlike older measurements providing only average neutron multiplicities the NESSI collaboration has very successfully extended

*Corresponding author: Tel.:+49-(0)2461-615232, e-mail: d.filges@fz-juelich.de

experimentally the available information by the eventwise measurement of the neutron multiplicity dM_n/dN [2] (and references therein) for different incident proton energies, various target materials and a large number of different cylindrical target geometries using a high efficient 4π gadolinium loaded scintillator detector [3].

The second share will concentrate on the energy deposition mechanism of high intensity proton pulses incident on target materials.

Precisely such systematic data—representing strong constraints on model calculations and at the same time providing a heavyset matrix of benchmark data are urgently needed to validate or/and improve high energy transport codes. This validation in turn is mandatory, since e.g. the optimization and the design of geometrically expendable high power target stations will finally rely on general Monte-Carlo particle transport codes having maximum predictive power.

In the present contribution the accent is put on the theoretical predictions obtained by the application of different high energy program suites such as the HERMES, MC4 [4,5], LCS [6] or MCNPX [7]. Experimental results from both experiments [2,9,10] will be confronted with these MC-models. Alternative to these BERTINI based intra-nuclear cascade (INC) codes we implemented the Liege INC code [8] in the latest version of MC4. This endeavor was necessary, because on one hand the independent Liege model could not describe the transport of particles in thick targets. Instead so far it has usually been applied as a stand alone code using a forced collision mode. On the other hand the Liege model emerges as a very reliable INC code for thin targets as far as excitation energies and production cross sections of charged particles and neutrons is concerned. At the same time the new approach is giving rise to further parameters as for example the switching time from INC to evaporation or the very fundamental variable of the nuclear radius r_0 being much smaller in the Liege model than in the BERTINI based codes.

II. COMPARISON BETWEEN EXPERIMENT AND MC-APPROACH

A study was performed in order to investigate the predictive power of the combination of various codes by intercomparing theoretical models and confronting the different approaches with experimental results [2,9,10]. We will outline the influence of important parameters optionally chosen in the models and finally point out some possible deficiencies in the models which shall be amended. While the production of neutrons is generally well described over a broad range of incident energies and different target geometries, there are big discrepancies with experimental data and among the different codes themselves when looking at the charged particle production cross sections in thin targets. Due to the multitude of possible interlinkings of these models and the plurality of adjustable options and parameter within these codes here only a representative selection is executed. This repertory however convinces already of the describability of the complex circumstances regarding neutron production in thick targets. In the following for LCS/MCNPX and HERMES a "standard" set of parameters was applied. The RAL evaporation-fission model [14] and the HETC level density have been selected. In addition the cutoff parameter for particles escaping during INC phase was set to 7 MeV. If not differently specified in the following all calculated observables will include the correction for the precise detector response, respectively. The details of both experimental setups can be found elsewhere [2,9,10].

A. The NESSI experiment

1. Reaction cross section and hadronic interaction length

For measurements using the 4π neutron detector BNB [3,2] and thick targets of the order of several cm in diameter and length the key observables are the neutron multiplicity M_n (measured eventwise!) and the reaction probability P_{reac}. Since we are counting all incident protons and the BNB provides also a prompt light signal with a rather low energy threshold (2 MeVee) even without the emission of any neutron, we are able to specify not only the neutron multiplicity per reaction, but also per incident proton—or P_{reac} related to the inelastic reaction cross section.

The hadronic interaction length for Pb, Hg and W following the MC-approach correspond with the experimental values [2] of $10.84 \pm 0.2, 15.06 \pm 0.3$ and 18.00 ± 0.3 cm, respectively. The experimental

reaction cross section σ_{reac} as deduced from 1-P_{reac} amounts to $\sigma_{reac} = 1.46 \pm 0.03, 1.64 \pm 0.05$ and 1.69 ± 0.03 barn as compared to calculated values (HERMES) of 1.62, 1.71 and 1.73 barn for W, Hg and Pb, respectively. This eminent conformity is confirmed also by calculations using the LCS2.70 or MCNPX code and shows that the observable σ_{reac} is well under control.

2. Neutron multiplicities

The average number of neutrons produced per incident proton M_n/p can be derived from the independently measured product of the reaction probability P_{reac} and the mean number of neutrons per inelastic reaction $\langle M_n \rangle$. Representative as a function of target length and for the two energies 1.2 and 2.5 GeV Fig.1 shows M_n/p for Hg, Pb and W. The solid line presents the HETC+MORSE calculation using the RAL evaporation model, $B_0 = 10$ for Pb, $B_0 = 8$ for Hg and W, option fission and elastic scattering switched on. After considering the detector response the theoretical prediction (dashed line) agrees completely with the experimental data (symbols) over a broad range of geometries, target materials and incident energies. The observed shift towards higher M_n/p for thicker targets is related to the increase of $\langle M_n \rangle$ due to secondary reactions and the increase of P_{reac} with target thickness.

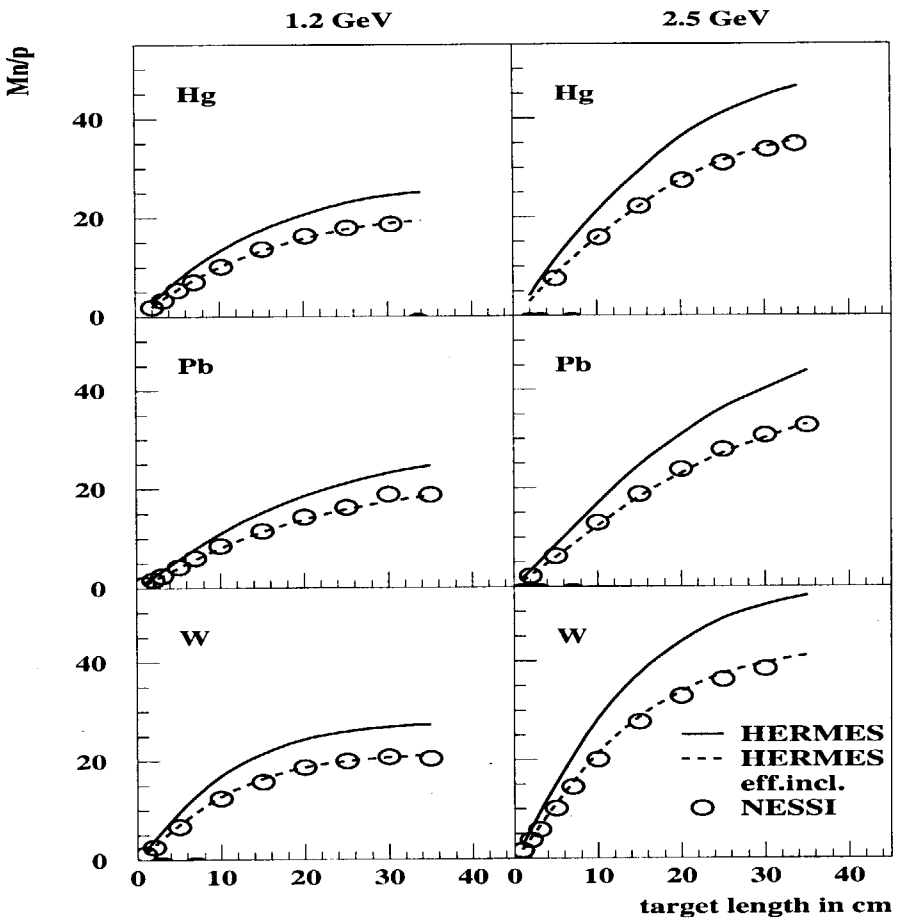

FIG. 1. *Average neutron multiplicity produced per incident proton M_n/p as a function of target thickness (diameter 15cm) for 1.2 and 2.5 GeV p+Hg, Pb and W. Solid line: HETC+MORSE, dashed line: HETC+MORSE with detector efficiency taken into account, o: NESSI exp.data.*

In contrast to previous measurements the event-wise character of the experiment NESSI allowed to gain access even to the distributions dM_n/dN rather than average values only.

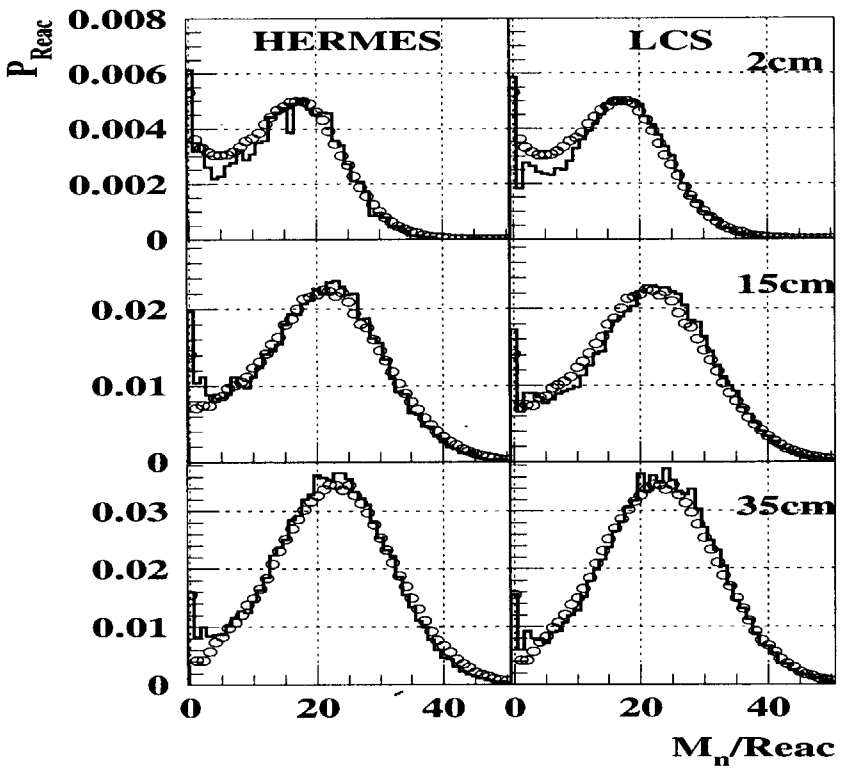

FIG. 2. *Neutron multiplicity distributions following the reaction 1.2 GeV p+Pb for different target thicknesses (diameter 15cm). Histograms: HETC+MORSE(left) and LCS2.70(right), ∘: NESSI exp.data.*

As a general tendency for all incident proton energies and target geometries the model predictions are in good agreement not only as far as the absolute values, but also the shape of the M_n-distributions is concerned as demonstrated in Fig.2. For all codes under consideration the deviation between experiment and model for P_{reac} and $\langle M_n \rangle$ is well below 8% except for peripheral reactions (low neutron multiplicity) on thin targets, where large deviations are obvious. The decrease of the latter deviations are due a compensation effect to be discussed below.

3. Deficiencies and particular variations within the codes

The previous section documented a very good general agreement between experimental and calculated neutron multiplicities and reaction cross sections for thick targets. If one decouples however the entire transport of the whole particle ensemble within thick targets and regards the primary reaction (one single nuclear reaction in thin targets) and specific decay channels (protons, neutrons, π,...) separately, then serious inconsistencies not only between experiment and simulation, but also among the codes themselves show up. This already indicates a kind of compensatory effect or redistribution of the total available energy in thick as compared to thin targets.

More specifically it is obvious e.g. that using BERTINI-like intra-nuclear cascade codes [12] we observe thermal excitation energy distributions *in thin targets* which are extending to larger values than the distributions of the INCL2.0 [8] calculations do for the same incident proton energy—as demonstrated in Fig. 3.

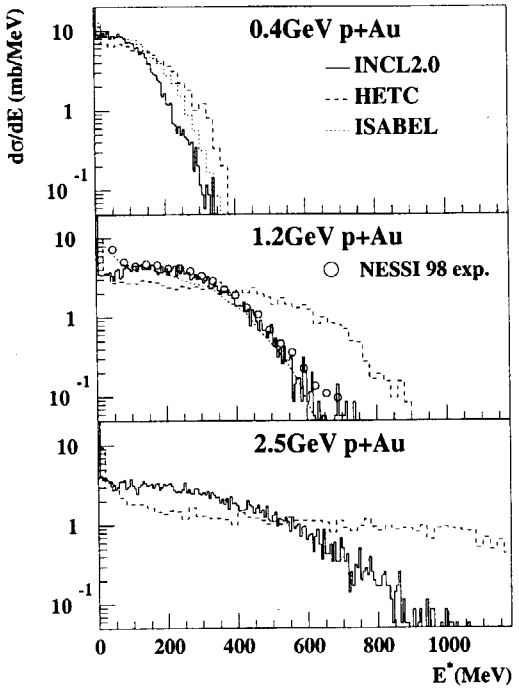

FIG. 3. *E*-differential cross-sections for 0.4, 1.2 and 2.5 GeV p+Au reaction following HETC, INCL2.0 and the ISABEL code.*

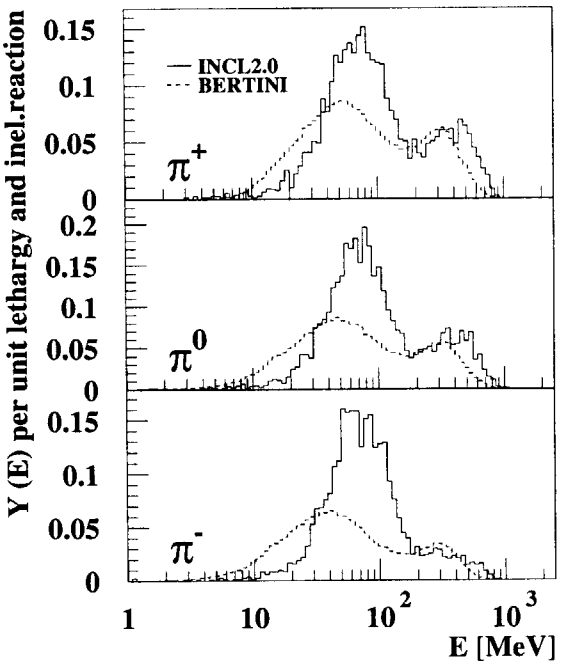

FIG. 4. *Kinetic energy spectra of $\pi^{\pm}$ and π^0 per unit lethargy following an inelastic reaction of 1.2 GeV p on Au for INCL2.0 and HETC codes.*

For the cut-off conditions determining equilibration standard parameters have been taken, respectively. ISABEL [13] and INCL2.0 calculations have been normalized to the reaction cross section of 1688 mbarn which is widely independent on incident proton kinetic energy.

Confronting $d\sigma/dE^*$ with experimental distributions [9] an almost perfect agreement can be obtained only with the INCL2.0 and ISABEL approaches. The BERTINI based codes fail to predict $d\sigma/dE^*$. On the average for large incident proton energies the BERTINI codes predict almost a factor of two higher E^* values than INCL2.0 does.

The considerable deviant between BERTINI on one hand and INCL2.0/ISABEL on the other hand for higher E^* is all the more pronounced the larger the energy of the incident proton is.

One assertion which could explain the disagreement is the way the originally transfered energy is being exhausted. While the INCL2.0 code predicts many relatively high energetic particles during the INC, the HETC codes (LAHET or HERMES) produce not only fewer, but also less energetic particles as shown representatively in Figure 4 for $\pi^{\pm}$ and π^0 production following the reaction 1.2 GeV p+Au. All pion kinetic energy distributions shown in Fig.4 are based on the same inelastic reaction cross sections of 1688mb. While conserving the total incident energy in all codes, it is obvious that during the INC the originally transfered energy is partitioned differently between E^* and the sum of kinetic energies and multiplicities of emitted particles or $\sum_{\pi^0,\pi^{\pm},p,n} E_{kin} + \sum_{\pi^0,\pi^{\pm}} m_{\pi} \cdot c^2$. As a matter of energy balance for BERTINI at the expense of larger E^* the quantity $\sum_{\pi^0,\pi^{\pm},p,n} E_{kin} + \sum_{\pi^0,\pi^{\pm}} m_{\pi} \cdot c^2$ is smaller than for the INCL2.0 approach. Since the pion model implemented in HERMES and LAHET is essentially the same, the kinetic energy spectra and pion multiplicities predicted by these codes coincide perfectly. Note also that evidently the pion spectra show a shift of the π^+ energy distributions compared to the π^- distributions due to the effects of the Coulomb field of the nucleus on the emitted pions.

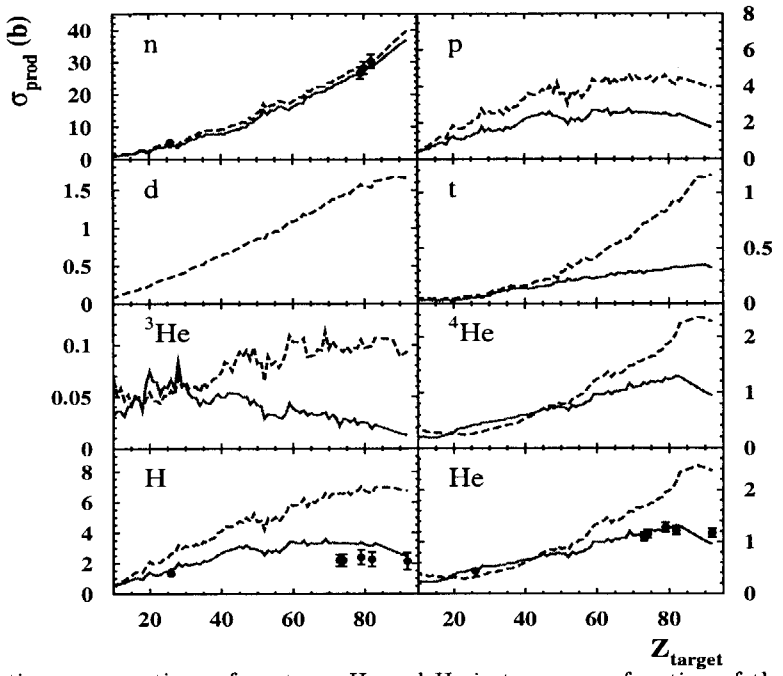

FIG. 5. Production cross sections of neutrons H- and He isotopes as a function of the atomic number Z following the bombardment of 1.2 GeV protons.

As a consequence of the extremely high thermal excitation energy E^* in the BERTINI based codes (in addition to deficiencies in the evaporation codes) also the particle production cross sections are overestimated. This applies especially to charged particles p, d, t and α, because they are subject to the Coulomb barrier and therefore preferentially emitted form high excitation energies. As shown by [9] for 1.2 and 1.8 GeV proton induced reactions on a variety of thin targets (mg/cm^2) ranging from Fe to U the production cross sections for H (all targets) and He (for heavy targets) isotopes are overestimated by a factor of two for BERTINI based codes, while the INCL2.0 code coupled to the statistical evaporation model GEMINI [11] gives reasonable agreement with the NESSI experiment as representatively demonstrated in Fig.5 for 1.2 GeV proton induced reactions.

The question whether these different multiplicities and energies are a matter of the different basic approach or whether different fundamental cross sections in the INCL2.0 code—enabling a dissenting production mechanism are responsible can currently not yet be answered.

B. The energy deposition experiment

As already mentioned next generations spallation neutron sources [1,15,16] will have proton beam power between 1 MW and 5 MW in 1μs pulses of up to 100 kJ/pulse. Liquid mercury has been selected as first priority material for the next generation spallation targets in Europe, Japan, and the United States. The container material for the liquid mercury will be subject of high radiation damage, high thermal mechanical load and corrosion by the liquid metal. Computer calculations show that, because of high thermal mechanical load tensile stresses may occur in the container. Therefore, it is essential to understand in great detail the energy deposition mechanisms of high intensity proton pulses incident on target materials. Since spatial distribution and intensity of the energy deposition are initial values for the thermodynamic calculations, it has also influences on: - the design of the target container, like mechanical stability, flow dynamics of the liquid metal and optimization of the cooling; - the request at structure materials, like behavior in relation to strong temperature gradients, fatigue strength, corrosion resistance; - and the life time of the target; Reliable prediction of the distribution and intensity of the energy deposition in the target presuppose an accurate simulation of particle production, particle transport and energy deposition mechanisms. Since the rise in temperature produced in the target is caused mainly as a consequence of ionization processes of charged particles the power density in the target can be determined via measurement of this processes. We applied the proton beam of COSY FZ Jülich with 0.8 and 1.2 GeV to mercury and lead targets of 15 cm diameter

and 35 cm length, which were equipped with 200 TL-detectors. The measured energy distributions were compared with detailed Monte Carlo calculations using the HERMES code system [4,5]. In the framework of the ASTE collaboration (AGS-Spallation-Target-Experiment) [17] the energy deposition and the temperature rise in the target during a proton pulse train of 24 GeV incident energy and a deposition power of 30 kJ per pulse were also investigated.

1. Theory

Charged particles lose their energy during the passage through material mainly by inelastic scattering at the atomic shell and by ionizing the atoms. The Bethe-Bloch formula serves to describe the mean energy loss dE of a charged particle by ionization on a distance dx. To draw conclusions from a dose measured in the detector material on the energy deposition in a spallation target the different stopping power of a charged particle related to the material must be considered. The quotient of the stopping power of the target material and the detector material serves to convert the dose in CaF_2 to the dose of the target material. Fig. 6 shows the stopping power for protons in the target material (Hg) and detector material as function of the proton energy. The ratio of stopping power from Hg and CaF_2 approaches in the area relevant for the measurements above 20 of MeV kinetic energy of the particles against a constant value. Due to this behavior of the quotient the measured dose in CaF_2 can be transferred to the target material.

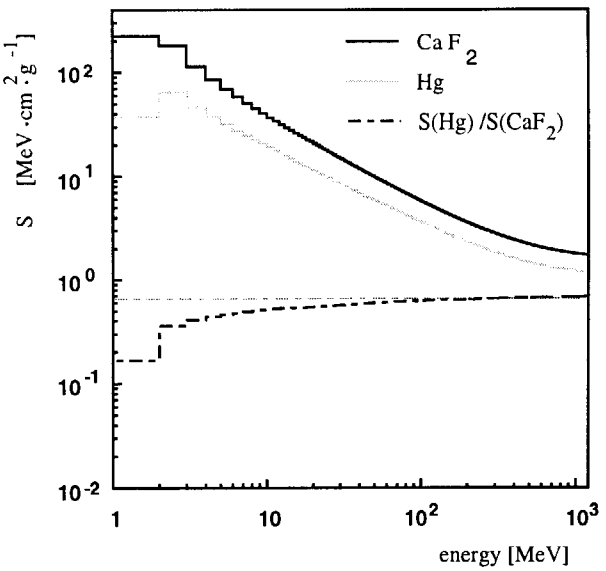

FIG. 6. Proton energy dependent stopping power S in CaF_2, Hg, and their stopping power quotient

2. Energy deposition experimental set up

For the measurements CaF_2:Tm detectors from Harshaw were used with a chip size of $0.3 \cdot 0.3 \cdot 0.1\text{mm}^3$. The dose response of the used TLD is linear in protons -, He^{2+}-, Ne^{10+} -, and in π^--fields up to a linear energy transfer ($\bar{y}_D$) smaller than 30 keVμm^{-1}, or 70 keVμm^{-1} [18]. The detectors are not sensitive against neutrons.

Measurements were executed with incident proton beam energies of 0.8 GeV and 1.2 GeV on lead and mercury targets. Fig. 7 shows the set-up of the mercury target and the position of the detectors. The Hg target material was in containers of 15 cm diameters of different thicknesses. The target length amounted to 35 cm.

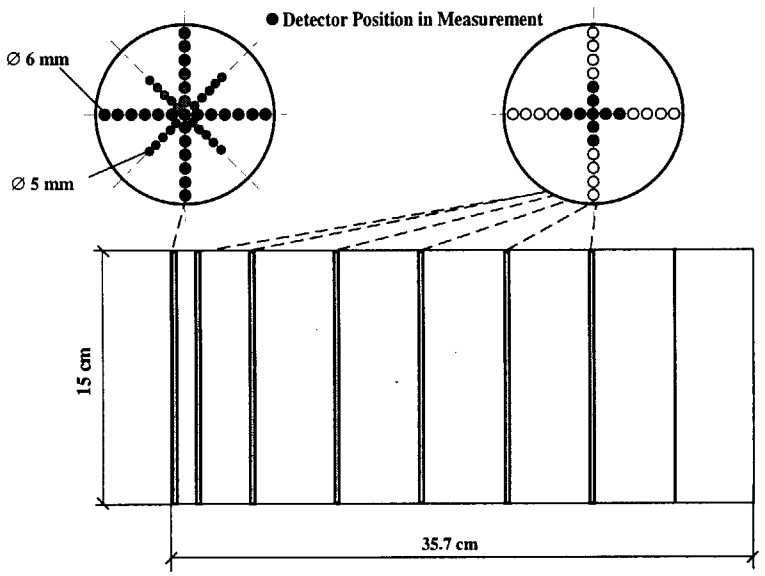

FIG. 7. Geometry of the Mercury Target

The detectors were positioned between the target segments by a position-disk of 1mm thick stainless steel. The first disk was equipped with 73, all following with 33 TL detectors.

In the first experiment at the mercury target with 1.2 GeV protons the TL position-disk in front of the the target was equipped with 33 detectors along the vertical (y axis), the horizontal (x axis), and the 45°-axis. The discrete measured values on the x and y axis were fitted with a gaussian function to optain a continuous intensity distribution to determine the beam profile intensity used for the simulations. The measured values of the x-axis and y-axis corresponded good to the applied values of the Gauss function. It was assumed that a superposition of the two gaussian distributions present the distribution of intensity in the xy-plane in the form: $f_{(x,y)} = af_{(x)}f_{(y)}$ Fig. 8 shows the comparison of the measured values to the 45°-axis and the assumed gaussian fit.

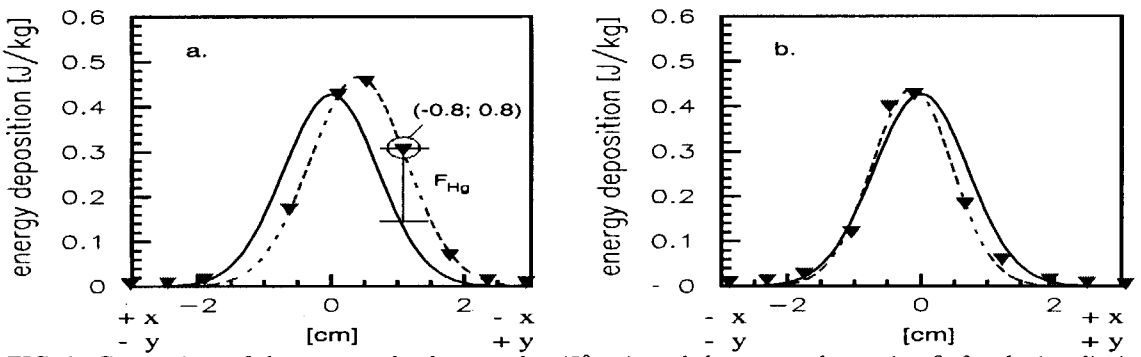

FIG. 8. Comparison of the measured values on the 45°-axis and the assumed gaussian fit for the irradiation of the mercury target with 1.2 GeV protons. Explanations see text.

For the measured point x=-0.8, y=0.8 the error resulting from the assumed function f_{hg} is shown as an example. Related to the measured value the assumed function indicates $f_{(x,y=x)}$ an error of 63%. The deviation of the measured values in relation to the assumed function $f_{(x,y=x)}$ is caused mainly by a shift of the maximum by 0.4 cm. This deviation is situated however in the context of the measurement inaccuracy, which results from the position of the TL detectors in the measurement. Under this aspect the approximation in the simulation, specified above, could be used.

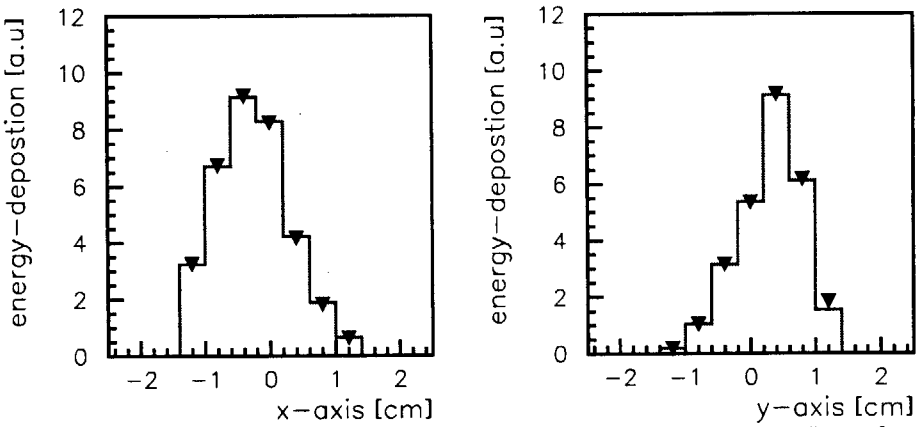

FIG. 9. Measured (Triangle) and Simulated (Line) Intensity Distribution of the Proton Beam for the Irradiation of the Lead Target with 1.2 GeV Protons

In additional irradiation experiments using a lead target a higher spatial resolution of the distribution of intensity of the proton beam could be obtained, because of a new position-disk. The distribution of intensity of the proton beam could be mapped completely by the TL-detectors, which cover an area of $2.8 \cdot 2.8$ cm^2. This enabled the application of a simulation method, which simulated accurately the measured distribution of intensity. With the help of a special developed source particle generator (SPG), implemented in the HERMES, any source distribution can be produced. The response is shown in Fig. 9. The filled triangles indicate the measured distribution of intensity and the line the simulated ones.

3. Results of energy deposition issue

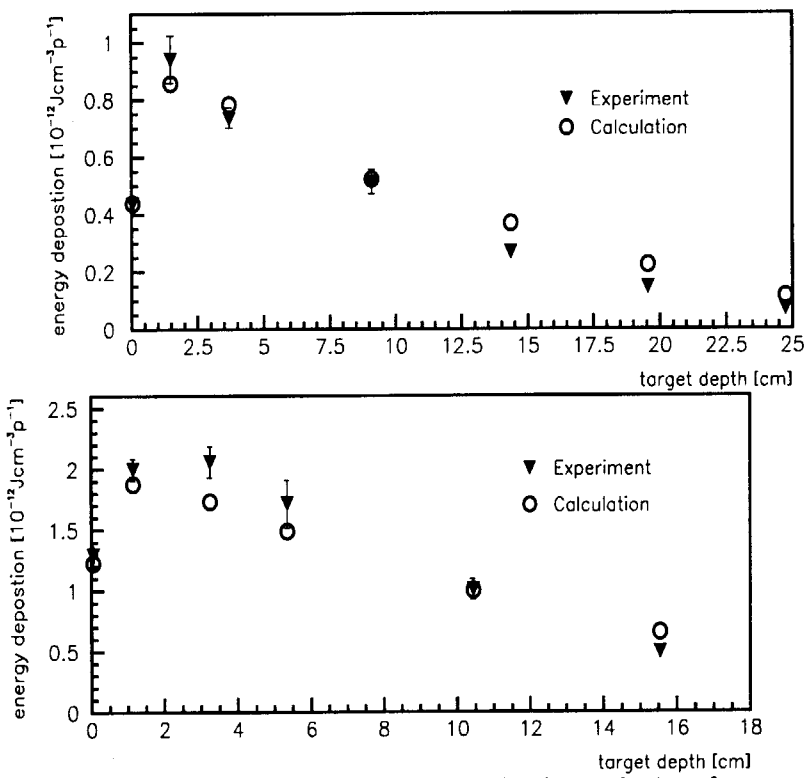

FIG. 10. Distribution of the energy deposition along the z-axis for the irradiation of mercury target (above) and lead target (below) with 1.2 GeV protons.

The axial energy deposition can be described by the following features:

1. The energy deposition in the target window, which produces thermal load must be considered for the design of the containment.
2. Value and position of the peak-energy deposition in the target parameters determine the pressure gradient in a liquid target material.
3. Shape of the function of energy deposition along the z-axis of the target

Fig. 10 shows the measured and simulated distribution of the energy deposition along the z-axis of the mercury and lead target irradiated with 1.2 GeV protons. The triangular marks indicate the measured values, the circles the simulated results. The first position (z=0) indicates the energy deposition normalized to stainless steel in the target window. All further results were normalized to the target material. For the both simulations the contribution of protons, deuterons, tritons, helium, pions, muons and recoils to the energy deposition were estimated. The simulations correspond good with the measurement. They underestimate the maximum of energy deposition in the target. With increasing depth the energy deposition is slightly overestimated. The measured values, the results of the simulation (Calc.) and the deviation of the simulation related to the results of measurement (Exp.) are represented in Tab. II B 3. The absolute agreement between simulation and experimental results is fairly well. For the Hg-target the peak deposition on z-axis is slightly underestimated by the simulation whereas the tails of the distribution along the z-axis is slightly overestimated. The accuracy between simulation and experiment is in the order of 5-10 percent. We are concluding from the results of the validation of the experiments that the predictive power simulating energy deposition in mercury and lead spallation targets is sufficient and accurate to supply reliable parameters for the engineering layout.

TABLE I. Comparison of Measurements (Exp.) und Simulation (Calc.) of the energy deposition along z-axis for Hg and lead targets with incident proton energy of 1.2 GeV* Normalized to stainless steel, ** Normalized to target material

Proton Energy 1.2 GeV						
Tar. Pos. z-axis [cm]	Exp. [10^{-12}Jcm^{-3}p^{-1}]		Calc. [10^{-12}Jcm^{-3}p^{-1}]		Calc./Exp.	
	Hg	Pb	Hg	Pb	Hg	Pb
0.05*	0.436	1.29	0.438	1.24	1.00	0.96
0.05**	0.751	1.86	0.754	1.79	1.00	0.96
1.50	0.940	2.00	0.857	1.91	0.91	0.96
3.70	0.732	2.06	0.784	1.78	1.07	0.87
9.15	0.512	1.72	0.522	1.54	1.02	0.90
14.35	0.268	1.00	0.368	1.03	1.37	1.02
19.55	0.146	0.49	0.224	0.67	1.53	1.36
24.75	0.070	-	0.114	-	1.64	-

C. Conclusion

The superior aim of the current contribution was to revise and improve the predictive power of nuclear reaction models for spallation source relevant data and the extension of INC/evaporation-codes with improved physics. A multitude of nuclear model calculations has been performed and compared to latest benchmark experiments. The NESSI experiment as well as an energy deposition experiment at COSY Jülich have been consulted to validate models with regard to reaction cross sections or reaction probabilities, neutron production cross sections and multiplicity distributions following proton induced reactions on thick Hg, Pb and W targets in a broad range of incident energies.

Due to the large variety of options, parameters, and–to some extend–liberties in the various models it is almost impossible to judge the quality of the codes in respect to all observables. Both the HERMES code system and the LCS or MCNPX packages master generally the prevision of neutron production in thick (and thin!) targets for a wide spectrum of incident energies and geometrical shapes of the target. All code packages convince of the describability of the complex circumstances regarding neutron production and energy deposition of the incident proton in thick targets. The predictive power of reaction probabilities and neutron multiplicities or neutron multiplicity distributions is almost perfect for the HERMES code for all target materials under consideration (Hg, Pb, W), but shows–especially for LCS and MCNPX–some weaknesses in the high incident energy domain (2.5 GeV) for dense targets like tungsten.

The complete implementation of a modern INC approach in MC4 is waiting for the latest release of the Liege (INCL3.0) code which is supposed to describe the excitation energy distributions and, as a consequence, the charged particle production cross sections superior than the BERTINI based INC codes.

Finally we pinpointed some possible deficiencies of the models essentially related to presumably too high thermal excitation energies in the BERTINI model. Also in the appended RAL fission/evaporation model Coulomb barriers are found to be underestimated. Even though in respect of such discrepancies the emission of charged particles in thin targets is drastically affected, the final abundance of neutron production in thick targets is accurately described.

The energy deposition is sufficiently well described by the codes for proton induced reactions on Hg and Pb targets in the energy regime relevant for spallation sources.

The deficiencies are identified in the present contribution and shall be amended in future releases of high energy transport codes. Although the state-of-the-art of computational models is sufficient in many cases for assessing spallation source/target systems performance, further "benchmarks" between users, experimentalists and code developers should be done in order to still improve the predictive power of nuclear reaction models.

ACKNOWLEDGMENTS

This research is partly supported by the TMR Program of the European Community under Contract No.: FMRX-CT98-0244, the German Helmholtz-Strategy Fonds and the French program GEDEON.

---

[1] The European Spallation Source Study ESS, vol III, The ESS Technical Study, report ESS-96-53-M, ISBN 090 237 6659 Nov.96, (1996)
[2] A.Letourneau et al., Nucl.Inst.&Meth.B, in press (2000).
[3] J.Galin, U.Jahnke, Nucl.Part.Phys. 20, 1105 (1994).
[4] G.Sterzenbach et al., 2nd International Topical meeting on nuclear App. of Acc. Technology, AccApp98', Getlinburg, Sep. 20–23, 1998, ISBN 0-89448-633-0.
[5] P.Cloth et al., HERMES, Report Juel 2203, ISSN 0366-0885, May 1988.
[6] R.E.Prael et al., User Guide to LCS: The LAHET Code System, Los Alamos National Laboratory, Report LA-UR-89-3014, Sep. 1989.

[7] H.G.Hughes et al., MCNPX–The LAHET/MCNP Code Merger, Resaerch Note XTM-RN(U)97-012, LA-UR-97-4891, Los Alamos National Laboratory (1997).
[8] J.Cugnon et al., Nucl.Phys. A470, 558 (1987).
[9] M.Enke et al., *Nucl.Phys.* A, Volume 657, 317 (1999).
[10] A.Tietze, PhD-thesis, University of Wuppertal (2000).
[11] R.J.Charity et al., Nucl.Phys. A483, 371 (1988).
[12] H.W.Bertini et al., Phys.Rev. 134, 1801 (1963).
[13] Y.Yariv et al., Phys.Rev.C 20, 2227 (1979).
[14] F.Atchison et al., Proc. of a specialists' meeting, Intermediate Energy Nuclear Data: Models and Codes, Issy-les-Moulineaux (France), May 30–June 1 (1994).
[15] J.R. Haines et al., Overview of the Target Systems for the Spallation Neutron Source (SNS) Proc. of the 2nd Topical Meeting on Nuclear Applications of Accelerator Technology, AccApp'98, Sept. 20-23, 1998, Gattlingburg, USA, pp. 222-229.
[16] S.Nagamiya, JAERI-KEK Joint Project on high Intensity Proton Accelerator, 9th Int.Conf. on radiation shielding, Oct 17-22nd, 1999, Tsukuba, Japan.
[17] D.Filges et al., Experimental Validation of Nuclear Models for the Optimisation of the ESS Target System. Proc. of the 2nd Topical Meeting on Nuclear Applications of Accelerator Technology, Sept. 20-23, 1998, Gattlingburg, USA, pp. 28-31
[18] W.Hoffmann et al., Radiat. Prot. Dosim. 85, 341-343(1999)